Heat Transfer Characteristics of Plate Fin Heat Sink with Longitudinal Vortex Generators

Structured Abstract

Purpose:

This article aims to provide an insight into the relationship between design parameters and thermal performance of plate-fin heat sinks incorporating longitudinal vortex generators inside a plate fin heat sink channel.

Design/Methodology/Approach:

A computational fluid dynamics model of a delta winglet pair vortex generator mounted inside a plate-fin heat sink geometry is detailed, and the model is validated by comparison with experimental data. The validated model is used to perform a virtual design of experiments study of the heatsink with bottom plate and vertical plate mounted vortex generators. Data from this study is used to regress a response surface enabling the influence of each of the assessed design variables on thermal performance and flow resistance to be determined.

Findings:

The results show that the thermal hydraulic performance of a plate fin heat sink with bottom plate mounted vortex generator and vertical plate fin mounted vortex generator are respectively 1.12 and 1.17 times higher than the baseline plate fin heat sink. Further the performance variation of the heat sink with vortex generator, relative to delta winglet's arrangement (common flow up and common flow down), trailing edge gap length and Reynolds number were also evaluated and reported.

Originality/Value:

1

For the first time, performance characteristics of delta winglet vortex generators mounted inside the plate fin heat sink is evaluated against different design variables and a polynomial regression model is developed. The developed regression model and computed results can be used to design high performance plate fin heat sinks mounted with delta winglet vortex generators.

1. Introduction

Heat sinks are widely used in the micro-electronics industry to dissipate the heat generated from integrated circuits and other devices. The increasing desire for miniaturization and increasing levels of power density, demand much higher cooling capabilities from the heatsinks. Plate fin heat sinks (PFHS) are widely used in microelectronics thermal management. PFHS typically have several thin plate fins kept along the flow direction. To increase the cooling capability of heat exchangers and heat-sinks, dimples, holes and roughness are introduced onto the fins. Alternatively, heat transfer of heat sinks can be improved through the addition of vortex generators (VG), intended to generate longitudinal vortices in the heat sink channel. The vortices increase the exchange of hot and cold fluid on the fin surfaces thereby will increase the heat transfer. Currently extensive research is going on to utilize the VGs to increase the heat transfer.

Studies on the use of VG to increase the heat transfer was there for long time. Fiebig et al. [1] were the first to study the performance of longitudinal VG on a rectangular channel experimentally. The results showed that local heat transfer was increased by 200% and Colburn factor was increased from 20 to 60%. They have considered different VGs, namely delta winglet pair and rectangular winglet pair, which were punched from the bottom flat plate. Since the VGs were punched, there was a hole in the bottom wall. Highest heat transfer enhancement was reported by delta wings, followed by delta winglets and rectangular winglets. The best location for winglet type VG on fin and tube heat exchanger, is found to be at 50% of the tube diameter in both streamwise and spanwise direction [2].

Reference [3] numerically studied longitudinal VG on a laminar rectangular channel and found that Nusselt number (Nu) decreases as VG is moved away from the inlet, and as the

distance between the VG pair is decreased. Increasing the length of VG will enhance heat transfer more than increasing the height, without significantly impacting on the flow loss. For the same surface area, delta winglet pair is more beneficial than the rectangular winglet pair. Effect of the longitudinal VG on the heat transfer of both surfaces (upper side and lower side) of one fin in a fin-and-tube heat exchanger was studied by [4]. If the vortex generating winglets are arranged in such a way that spanwise distance between leading edges are much higher than spanwise distance between trailing edges then this arrangement is called Common-flow-up (CFU). On the other hand, if, distance between trailing edges are higher than distance between the leading edges then it is common-flow-down (CFDN) arrangement.

He et al. [5] worked on rectangular winglet mounted on fin-and-tube heat exchanger and found that pressure drop penalty due to winglet vortex can be decreased by opting for staggered VG arrangement instead of inline arrangement. Further study [6] on fin and tube heat exchanger with inline row of tubes and staggered row of tubes with rectangular pair VG has shown that, the nozzle like flow acceleration effect created by VGs are more pronounced in inline tubes than in staggered tubes. This leads to increased heat transfer benefit in inline tube arrangement. Sinha et al. [7] studied the effect of different orientation of two rows of winglet arrays on plate fin heat exchanger. The results showed that CFU followed by CFU rows of VG have performed better than other configurations. Zhou [8] investigated plane and curved winglets with punched holes. He found that curved VGs are better than plain VGs and the holes on the VG improve the thermohydraulic performance.

Aliabadi et al. [9] evaluated the effect of rectangular wing type transverse VGs on plate fin heat exchanger channel using 3-dimensional computational fluid dynamics (CFD). Based on the study results, correlations for Nu were derived. The results also showed that wing height and

wing attack angle were influential parameters than other parameters. Performance of different delta winglet VG inserts in a circular tube was experimentally studied in [10] using water as the working fluid. Different VG configurations were studied and found that maximum performance evaluation criterion of 1.41 is obtained for the best VG configuration. Researchers have also used genetic algorithm and neural network to maximize the heat transfer from rectangular channels based on geometric variables of VG [11, 12]. Apart from rectangular channels, VGs were also studied on triangular channels [13-15].

Wijayanta et al. [16] did experiments on punched delta winglets and studied the effect of attack angle on the heat transfer and friction factor performance of circular tubes. Results showed that Nu and friction factor had uptrend with attack angle and a maximum thermal hydraulic performance (THP) of 1.22 obtained for 70° attack angle. This work was extended with numerical simulations in [17]. Song et al. [18] carried out experimental studies on circular tube and fin heat exchanger with curved delta winglet VGs. Results showed that smaller VGs closer to the tube are advantageous for heat transfer. Reference [19] studied the effect of transverse distance between VGs on the interaction of longitudinal vortices and the heat transfer performance. The effect of transverse distance on co-rotating longitudinal vortices and counter-rotating longitudinal vortices are studied. Results showed that transverse distance has significant effect on the counter-rotating vortices than on the co-rotating vortices.

While most of the VG work is carried out on fin and tube exchangers and channel flows, few works are done on heat sinks [20-23]. Reference [20] examined the air side performance of heat sinks with fins having patterns like delta shape VG, semi-circular VG, plain fin and their combinations. The study found that, semi-circular VG's are effective at developing flow region. For the same pumping power and same heat transfer capacity, it was found that asymmetric

design of VG fin with plain fin produces best result. Li et al. [21] studied the effect of externally mounted delta winglet VG on the performance of PFHS. Results showed that attack angle of 30° is preferred. VG effect is better at lower Reynolds (Re) numbers and CFU is beneficial than CFDN configuration. Effect of external VGs on the pin fin heat sink was investigated in [22]. Ahmed [23] evaluated the effect of fixing ribs in PFHS in comparison to plain PFHS. Different geometric parameters of ribs were studied, namely, different rib size, locations and numbers. They also investigated how many fins can be reduced (material reduction) due to the performance improvement of VG ribs.

Yang and Chen [24] optimized the heat transfer performance of a two-dimensional channel with ribs using genetic algorithm-based optimizer. Results showed that staggered ribs increase the performance much higher than the inline ribs. Sharma et al. [25] evaluated the performance enhancement by pentagonal ribs on rectangular channels by conducting experiments using liquid crystal thermography to measure the surface temperatures. Results found that pentagonal ribs yield better thermo-hydraulic performance than the square ribs. Liu et al. [26] numerically and experimentally studied 4 different VGs mounted on the bottom wall of rectangular channel. Results showed that VGs increased the Nu up to 92% when compared with plain channels. Song et al.[27] studied the effect of convexity and concavity on the triangular VGs mounted on the bottom wall for laminar flows. They have also obtained correlation equations for Nu in terms of Re, central angle and other parameters. Ali et al. [28] studied the effect of multiple pair of VGs mounted on the rectangular channel and the results have shown that five pairs of VGs increase the heat transfer by 59% compared to plain channel.

Naik and Tiwari [29] studied the location effect of rectangular winglet pair VG on fin and tube heat exchanger. Angle of attack from 15° to 60° is also studied. From their study they found

the location of VG which will give maximum thermo-hydraulic performance. The characteristics of curved rectangular winglet placed in a channel was studied in [30]. Reference [31] studied VGs to enhance the heat transfer on fin and tube heat exchanger with various tube shapes (circular, oval and rectangular). The optimum attack angle of VG is found to be 165°. It is also found that staggered tube arrangement is better than inline arrangement and oval and circular tubes are better than rectangular tubes. Reference [32] studied the effect of pin fin on the straight and wavy miniature heat sinks experimentally and computationally. The results showed that, for the same pumping power, heat removal rate of heat sinks with pin fins are higher than the smooth heat sinks. The pin fins have shown to enhance the heat transfer coefficient by 0.17 to 1.95 times that of smooth heat sink configuration. Hosseinirad et al. [33] studied on the ways to reduce the flow separation and associated pressure drop of square pin fins, by using splitter plate attached with the pin fins at forward/rearward. Arched splitters extending forward of square pin fin is found to have lower base temperature than the other splitter configurations tested. Aliabadi et al. [34] studied the effect of co-current and counter current flow on the heat transfer characteristics of wavy mini-channel heat sink. Results showed that for the same pumping power, counter current flow lead to temperature uniformity and considerably increased performance index than the co-current flow.

 References [35,36] reviewed the heat transfer augmentation using VG considering both approaches and applications. Other novel methods to design heat sink with enhanced heat transfer are discussed in [37,38].

From the literature survey, we can determine that most of the VG research published has been conducted on tube-and-fin heat exchangers with little work carried out on PFHS. The previous studies conducted on PFHS have mounted the VG external to the PFHS, with the

exception of the work of [23], which studied ribs mounted on the bottom of heat sink channel. As the PFHS channel width is small, the VG needs to be smaller in size, like a micro-VG, to fix the VG within the channel. Mounting VGs within the heat sink channel will be more beneficial than mounting them outside and delta winglet VGs are more effective than ribs. Hence, in this study, delta winglet pair VGs are mounted inside the heat sink channel to enhance the thermal performance of PFHS by mounting them either on the bottom plate or on the vertical plate fins. Polynomial regression models are developed separately for the thermal performance of PFHS with bottom plate VG and vertical plate fin VGs. The effect of various VG design parameters, the effect of gap length between the delta winglet's trailing edge, the configuration (CFU or CFDN) effect and Reynolds number effect are also evaluated in this study.

2. Problem description

2.1 Plate Fin Heat Sink

PFHS are commonly used in the electronic industry to cool micro electronic devices (*Fig.* 1). As the power density rating of electronic devices are continuously increasing, there is a need to increase the cooling effectiveness of PFHS. As the cold fluid gets heated up while flowing through the channel, the cooling effectiveness of the PFHS is quite low at the rear portion of the plate fins. Many different concepts for improving the cooling effectiveness have been investigated in the past, with vortex generation being one of the most promising options. Longitudinal VGs create streamwise vortices in the downstream flow, enhancing the thermal mixing and increasing downstream heat transfer. The length to width ratio of the heat sink channels typically range from 10 to 15. The dimensions of the PFHS considered in this study are given in Table 1.

8

2.2 Vortex Generators

Most of the research on the use of VG for heat transfer enhancement has focused on fin and tube heat exchangers. Minimal research has been performed on PFHS and the research that did focus on this heat transfer approach, employed VG on the outside of the plate-fin channel. That is VG is mounted externally to the PFHS. This study focuses on cases where VGs are mounted inside, on the bottom plate and vertical plate fins.

While the addition of VGs increases heat transfer, this comes at the cost of additional drag, increasing the pumping power requirement. When parameterizing the design of the VG, we need to differentiate between the different VG types. Depending on the shape of the VG it can be classified as i) rectangular wing VG, ii) delta wing VG, and iii) delta winglet pair. Depending on how they are arranged in streamwise direction, the winglet pair can be in CFU configuration or CFDN configuration. In this study, delta winglet pair VGs are considered, as they were found to give better performance than others [3]. The winglet pair is arranged in CFU mode. Different design variables of delta winglet pair VG are, (i) Attack angle (α), (ii) Height of VG (h), (iii) Length of VG (L), (iv) Axial Location of VG (x) and (v)Gap between the winglet pair (g), which are shown in *Fig. 2*.

For the PFHS, the VG can be mounted either on the bottom plate or the vertical plate fins. In this study, the performance of the VG mounted on both these plates is evaluated. For the bottom plate VG (*Fig. 2*), design parameters like Height, Length, and x-location are evaluated. VG thickness is considered to be 0.2mm. The distance between the leading edge of winglet and plate fin (w) is considered to be 0.5mm (on both the side of the channel). The gap between the winglet's trailing edges (g) is considered to be 1mm. Since the flow is incompressible, lower the

9

exit gap (area) higher will be the exit velocity (Mass conservation) and the cooling capability. So a trailing edge gap of more than 1mm is not preferred as this will lead to lower cooling capability by the VGs.

For vertical plate VG, the effect of design parameters Height, Attack angle, Length, and x-location have been evaluated. A fixed gap (v) of 0.75mm has been left between the bottom plate and the leading edge of the lower delta winglet. Similarly, a gap of 1mm was maintained between the delta winglet trailing edges (*Fig. 3*). Response surface models for performance parameters Nu and THP were generated in terms of the design parameters for both bottom plate VG and vertical plate VG by carrying out a CFD based design of experiments.

3. Numerical simulation details

Jonsson and Moshfegh [39] performed experiments on various plate-fin heat sinks at velocities 8, 10 and 12m/s. All of these heat sinks were fully shrouded, and the top surface is insulated. The present numerical setup will be validated by comparing the results of [39]. Later Zhou and Catton [40] investigated the thermal and hydraulic performance of 20 different heat sinks using three-dimensional CFD. The computational domain used in this study are the same as that of [40].

3.1 CFD model

The three-dimensional numerical evaluations are planned to be carried out at velocities 8 to 12m/s. Flow is assumed incompressible and steady. The Reynolds number range corresponding to this velocity range, based on the pitch of the heat sink, is 2739 to 4108. This velocity range is chosen because the heat sink channel flow is created by mini fans and the air

velocity generated by them varies from 1 to 8m/s. Reynolds observed that transition from laminar to turbulence occurs at a Re of 2300 in a circular pipe, but the precise value of Re depends on the presence of disturbances. Further, Hank and Ruo [41] points out that transition Re for a rectangular channel with aspect ratio=2 is 1900. Heat sink channels of current study have an aspect ratio of 2. It could be noted that the flow generated by cooling fans are generally turbulent. So, the heat sink channel flow in the Re range of 2000 to 4000 is considered turbulent. To computationally model this flow, Reynolds Averaged Navier Stokes equations are solved with k-ω SST turbulence model. This turbulence model is more suitable for the calculation of wall bounded flows and it is more accurate and robust for flows with strong pressure gradients. Readers may refer to [42] for the details about k and ω equations. The mass, momentum, and energy equations are shown in Eq. (1-3), where u is the mean velocity vector and μ_t is turbulent dynamic viscosity, which is evaluated by solving k-ω shear-stress transport equations. Inlet turbulent intensity is considered as 5%. Radiation heat transfer was not considered in this study. The Fluent 18.2 commercial CFD solver was used to solve the flow physics. A second-order upwind differencing scheme has been used, with the SIMPLE algorithm coupling pressures and velocities in a manner that ensures continuity.

The working fluid is considered to be air with an inlet temperature of 294K, and the PFHS is considered to be formed from Aluminium. The material properties of Air and Aluminium are given in Table *2*. A constant heating power of 10W is considered. The conjugate heat transfer simulation is carried out by simultaneously solving for the heat transfer in the fluid domain (Eq. 1 -3) and solid domains (Eq. 4). In Eq.4, Q denotes the volumetric heating source in solid domain.

$$\nabla.(\rho u) = 0 \tag{1}$$

$$\rho(u.\nabla u) = -\nabla p + \nabla.\{\mu\{\nabla u + (\nabla u)^T\} - \mu_t\{\nabla u + (\nabla u)^T\}\} \tag{2}$$

$$\rho C_p u.\nabla T = \nabla.\{(k + \frac{C_p \mu_t}{Pr_t})\nabla T\} \tag{3}$$

$$Q = \nabla.\{(k_s)\nabla T \tag{4}$$

3.2 Computational domain and mesh details

The computational domain used by [40] is replicated in this study to model the baseline PFHS (*Fig*. 4). Only one channel with two adjoining plate fins were used to model the PFHS. The outer side of plate fins are assigned with symmetry boundary conditions, and the modelled plate fin's thickness is half of the actual plate fin's thickness. The flow velocity was specified at the inlet, and the top and bottom side of fluid domain was specified to have zero shear walls. The side surfaces were specified with symmetry boundary conditions, and the specified heat flux value was imposed at the bottom of the solid heat sink. Outlet is specified with zero pressure, pressure outlet boundary condition.

The mesh for the computational domain was generated in the Ansys workbench. The solid domain was discretized with tetrahedral cells, while the fluid domain was discretized with prismatic cells near the wall, followed by tetrahedral cells (*Fig*. 5a). In total, 14 layers of prismatic cells were maintained to calculate the high gradient boundary layer flow accurately. Average y^+ value on the heat sink surfaces is maintained as 1. The total mesh size for baseline PFHS was 5.77 Million cells, while a total of 6.1 million cells were utilized for the PFHS with the bottom wall VG and vertical plate fin VG. The simulation was considered to have converged when the change in temperature over the previous 100 iterations was less than 0.01K, and the mass imbalance was less than 1×10^{-7}(*Fig*. 6).

A grid independence study was carried out to estimate the mesh error with the results shown in *Fig*. 5b. The CFD simulations were carried out using three different meshes of size 2.56 million, 6.24 million, and 14.02 million to compute the grid convergence index (GCI) [43] on Nu and friction factor. Both Nu and friction factor have shown monotonicity with the mesh refinement. The GCI or error due to mesh on Nu of 6.24 million mesh was 1.156%, while the same on 14.02million mesh was 0.991%. Since only marginal reduction was obtained on the mesh error with the refined mesh, the 6.24 million cell mesh was considered to be appropriate. For the selected mesh, the GCI of friction factor was found to be 0.143%.

To evaluate and rank the various PFHS configuration with VGs, the heat transfer coefficient (HTC), Nu, friction factor, and THP parameters (Eq. (5-9)) were evaluated. The expression for THP (Eq.9) is based on the constraint of identical pumping power. Fan et al. [44] indicate that this performance index indicates heat transfer enhancement for identical pumping power. Readers may refer to [44] to find out suitable expression for the heat transfer performance parameter for identical pressure drop and identical flow rate constraints. Mass weighted averaging was used to calculate the temperature at inlet and outlet. Δp is the pressure difference between inlet and outlet required to maintain the flow. D_h is the hydraulic diameter of the channel and L_f is the length of heat sink channel. T_w is the area averaged bottom wall temperature and A_{HT} is the total area of heat transfer surfaces. To calculate Nu, the PFHS channel's length and air's thermal conductivity are used as references. THP is calculated by using the performance parameters of baseline PFHS (Nu_s, f_s) and PFHS with VG (Nu, f).

$$T_{ave} = \frac{(T_{out} + T_{in})}{2} \tag{5}$$

$$HTC = \frac{\dot{m}Cp(T_{out} - T_{in})}{A_{HT}(T_w - T_{ave})} \tag{6}$$

$$Nu = \frac{HTC.L_f}{k} \tag{7}$$

$$f = \frac{2.\Delta P}{\rho u^2}(\frac{D_h}{L_f}) \tag{8}$$

$$THP = \frac{Nu/Nu_s}{(\frac{f}{fs})^{1/3}} \tag{9}$$

3.3 Validation of CFD model

The numerical setup of this study was validated by evaluating the baseline PFHS performance at velocities 6.5 to 12m/s and by comparing these results against the experimental results of [39] (*Fig*. 7). Jonsson and Moshfegh [39] conducted wind tunnel test to evaluate the performance of heat sinks with 7 different fin types (including plate fins) in the Re range of 2000 to 16500. Temperatures are measured with type T thermocouples while pressures are measured with Autotran 700D pressure transducers. Based on the test results they developed correlations to predict Nu and dimensionless pressure drop. The experimental uncertainty reported by [39] on Δp measurement is ±0.61% (min) to ±30.4% (max) and the uncertainty on mean velocity is ±2.26%(min) and ±3.39% (max). It was reported that the large error (max) limits in pressure drop are due to the in-accuracy in measuring small pressure drops (Pressure drop smaller than 0.5Pa have been discarded in the measurement). The specified accuracy of thermocouples used for temperature measurement is ±0.5°C.

The validation shows that at 8m/s velocity, the difference between pressure predicted by CFD and experiment is 7.3%. Further, the CFD predicted Δp lies within the error bounds of

14

experimental values for all the velocities. Similarly, CFD predicted base plate temperature lies within ±0.5°C to experimental value except at velocity=6.5m/s. It should be mentioned that in the experiments, only 4 symmetrically placed thermocouple measurements were used to calculate the average base plate temperature, but in CFD, temperature of all the mesh points are used to calculate the average. So, the difference in averaging method and the uncertainty in the experimental velocity could have resulted in the noticeable difference in temperature at the velocity=6.5m/s.

3.4 Response Surface Modelling

A seventeen-point design of experiment (DoE) has been conducted for the bottom plate VG configuration with Latin Hyper Cube (LHC) sampling. The LHC sampling approach was selected because it provides the best coverage of the hypervolume defined by the bounds of the different design variables. The design parameters bounds of three design variables, for the bottom plate VG study are shown in Table 3. VG length was allowed to vary from 1.5mm to 6.5mm, and VG height is non-dimensionalized with respect to length of the VG, and maximum height can be equal to its length. The maximum length is limited to 6.5mm, as the height of the fin plate is 10mm. The thickness of the VG is considered as 0.2mm.

Similarly for the vertical plate fin VG configuration, a nineteen-point LHC sampling based DoE is carried out. For each point in the DoE, geometry and mesh are generated, and governing thermal equations are solved by CFD simulation. The height of the vertical plate fin VG was limited to 2.25mm (less than half of channel width) as the width of the channel is 5mm. It should be noted that delta winglet pair VGs are mounted on both the vertical plate fins. Attack angle was varied from 8° to 30° and the length of VG is varied from 1 to 6 times of VG height. In

both bottom plate VG and vertical plate VG, the delta winglet pair is arranged in CFU configuration and flow velocity is considered as 8m/s.

4. Results and discussion

By conducting CFD-based DoE simulations, characteristics of PFHS with bottom plate VG and PFHS with vertical plate fin VG are evaluated in terms of corresponding design variables. In addition to this, the effect of the gap between winglet trailing edges, comparison between CFU and CFDN VG configurations, and the change in PFHS with VG performance relative to velocity are evaluated and presented in this section.

4.1 Effect of gap length (g) between delta winglet trailing edges

In order to assess the effect of gap length between delta winglet trailing edges on the performance of the PFHS with bottom plate VG, two different gap lengths (1mm and 2mm) were considered (*Fig*. 2). While maintaining the other design parameters invariant, only the gap length is changed, and CFD simulations are carried out on these two configurations. The results show that VG with 1mm gap has 2.6% higher THP value and 9% higher Nu value than VG with 2mm gap (Table *4*). From the temperature and velocity contours (*Fig*. 8, *Fig*. *9*), reducing the gap increases the velocity on the vertical fins, leading to better convective heat transfer. Hence the wall temperature of the vertical fins of 1mm gap PFHS has decreased considerably than vertical fins of 2mm gap PFHS.

4.2 PFHS with bottom plate VG results

A seventeen-point DoE based on LHC sampling was completed to evaluate the effect of design variables namely, height of the VG, length of the VG and x-location of the VG. The gap length between delta winglet trailing edges is considered as 1mm, as it gives better performance than

the gap length of 2mm. Based on the CFD results, Nu, friction factor and THP parameters were evaluated. A polynomial response surface model (Eq. (10)) for the Nu and THP was developed which has linear, quadratic terms and interaction terms between the design variables. It should be noted that all the design variables are scaled to a normalized magnitude of range [0,1] before the response surface model was developed. The coefficient values of model equation are given in Table 5. R^2 statistic is a measure of how close the data are to the fitted regression line and is calculated based on Eq. (11). In this equation, y_i denotes the response variable (Nu) and $\hat{y}_i$ denotes the response value predicted by the fit and $\bar{y}$ is the mean of all response variables. R^2 values for Nu and THP models are 97.47% and 82.42% respectively. This indicates that Nu model has very good accuracy, while the THP model has reasonable accuracy.

$$Y = \beta o + \beta_1 L + \beta_2 h + \beta_3 x + \beta_4 L^2 + \beta_5 h^2 + \beta_6 x^2 + \beta_7 Lh + \beta_8 hx + \beta_9 xL \quad (10)$$

$$R^2 = 1 - \frac{\sum_i (y_i - \hat{y}_i)^2}{\sum_i (y_i - \bar{y})^2} \quad (11)$$

The results show that h= 0.2 to 0.6 will yield good THP values (*Fig*. 10). High h is not favourable for THP as this will increase the pressure requirements drastically. But for high Nu, height has to be higher. Higher VG length will provide higher Nu and higher THP values. The VG length can be correlated with the attack angle of the winglet. As length increases, attack angle decreases for the bottom plate VG arrangement, because of the fixed z-position of the VG trailing edges. As reported by other researchers, forward mounted VGs (VG with lower x/L$_f$ value) provide better THP performance than the aft mounted VGs. Among the three design variables, h is the dominant parameter, and this is indicated by the higher coefficient value of h term, excluding the constant term, β_o (Table 5). The model coefficient values indicate that there

is considerable interaction between any two design parameter combinations. The best performing bottom plate VG gives a THP increment of 12% compared to the baseline PFHS.

4.3 PFHS with vertical plate fin VG results

A nineteen parameter DoE study was conducted in order to evaluate the effect of design variables VG height, attack angle, length and x-location. Based on the CFD results, performance variables HTC, Nu and THP were evaluated. A polynomial equation with linear, quadratic and interaction terms was fitted for Nu and THP (Eq. (12)). These variables are scaled to a normalized magnitude range [0,1] prior to developing the response surface model. The coefficient values of the model equation are given in Table 6.

$$Y = \beta o + \beta_1 h + \beta_2 \alpha + \beta_3 L + \beta_4 x + \beta_5 h^2 + \beta_6 \alpha^2 + \beta_7 L^2 + \beta_8 x^2 + \beta_9 h\alpha \qquad (12)$$
$$+ \beta_{10} \alpha L + \beta_{11} Lx + \beta_{12} hx + \beta_{13} hL + \beta_{14} \alpha x$$

Based on the model, the variation of Nu and THP with respect to different combination of design variables at 3 different x-locations are given in *Fig*. 11 and *Fig*. *12* respectively. The results indicate that, either very low (close to zero) h or very high (close to 1) h is preferred for higher THP performance. More precisely, if the VG is fixed close to the heat sink's leading edge, then higher h is preferred but if the VG is fixed backward, then lower h values are preferred. While the former case improves the Nu, the latter case improves the friction factor, thereby improving the THP. It can also be observed that higher attack angles are required for higher THP performance. If VG location is forward (low x/L_f), a medium VG length can give better THP performance, but as x/L_f value increases, higher VG length is necessary for better THP performance. This indicates that the drop in performance due to high x/L_f can be compensated by

the increase in VG length or height, but this is possible until x/L_f remains less than 0.5. Comparison of model equations coefficient values show that, among the four variables, angle is relatively weak variable with less influence on THP than other variables. Simulations have shown that one of the best vertical plate fin VG configuration on PFHS provides a THP value of 1.17 times higher than the baseline PFHS. This THP improvement is higher than the improvement provided by the bottom plate VG (1.12 times). Hence fixing VGs in the vertical plate fin is more beneficial than fixing VGs in the bottom plate.

4.4 Comparison between CFU and CFDN VGs

The best performing vertical plate VG in CFU arrangement has given 1.17 times higher THP performance than baseline PFHS. Using the same delta winglets (same length, height and x-location) a CFDN VG pair is developed and fixed on the plate fins of PFHS (*Fig. 13*). Following the same meshing strategy, a new mesh is generated for the CFDN VG, and CFD simulation was also carried out. Comparison of the two configurations show that the CFDN configuration performs better than the CFU configuration (

Table *7*). The Nu of CFDN configuration is slightly higher, and the friction factor is slightly lower. It is observed that CFDN configuration requires a slightly lower pressure difference to maintain the same flow velocity. In CFDN configuration, trailing edges of delta winglets are well separated (along y axis), which gives some relief for the flow; hence pressure drop requirements are relatively lesser than CFU configuration.

To understand the heat transfer enhancement by the VGs, secondary flow generated by the VGs are analyzed. Primary flow or core flow is considered along the x-axis in this study. But the

presence of VG introduces a flow in the plane normal to the x-axis. This flow is called as

secondary flow and Song and Wang [45] introduced a parameter called 'secondary flow intensity

factor' Se to quantify the secondary flows (Eq. (13)).

$$Se = \frac{\rho D_h^2}{\mu} \left(\frac{\int_\Omega |\omega_n| d\Omega}{\int_\Omega d\Omega} \right)$$
(13)

Where D_h is the hydraulic diameter, $|\omega_n|$ is the magnitude of the vorticity, normal to the cross

section and Ω is the volume of the considered domain. Se is a non-dimensional number, which

represents the ratio between inertial force to viscous force, induced by the secondary flows. VGs

generate secondary flows and high value of Se results in high levels of heat transfer and Nu.

Secondary flow intensity averaged over a cross section (Se_{cs}) can be calculated using Eq. (14),

where A is the area of cross section.

$$Se_{cs} = \frac{\rho D_h^2}{\mu} \left(\frac{\int_A |\omega_n| dydz}{\int_A dydz} \right)$$
(14)

Cross section averaged secondary flow intensity factor for PFHS with CFU and CFDN

arrangement of VG are shown in *Fig. 14*. It shows that, CFU VG has a higher Se_{cs} peak, but at

the downstream its Se_{cs} value is lower than CFDN VG. The integrated value of Se_{cs} for CFU and

CFDN VGs are 216368 and 219584 respectively. The CFDN VG has higher integrated Se_{cs}

value and this leads to higher heat transfer by CFDN than CFU VG.

The two pairs of vortices produced by VGs are close to each other in CFU configuration, but the

vortices are vertically well separated in CFDN configuration (*Fig. 15*, *Fig. 16*). Further, the

CFDN VGs bottom vortices are so directed that they create a secondary flow normal to the

bottom plate, which is well aligned with the direction of the temperature gradient or heat flux. Based on the field synergy principle [46], heat transfer can be increased by reducing the angle between local velocity vector and temperature gradient vector. For this heat sink channel, heat flux vector acts normal to each of the three metal surfaces. The angle between CFDN VG's secondary flow and heat flux vector of bottom plate is zero (at mid-point), hence the heat transfer from the bottom plate increases significantly. This is indicated by the thermally mixed warm flow present near the bottom plate (Fig. *16*). Whereas the CFU vortices create secondary flow normal to vertical plates and hence will improve the heat transfer from the vertical plates. This is indicated by the thermally well mixed warm flow present at mid-height of the heat sink channel. CFDN VGs also create a secondary flow normal to vertical plate at the top of the channel, and this further improves the heat transfer from the heat sink.

As the VG trailing edges are vertically well separated in CFDN arrangement, the pressure drop required to maintain the flow is comparatively less. Whereas in CFU arrangement the VG trailing edges, where the vortices are generated are close to one another, this acts as a blockage to the incoming flow. So, more pressure is required to maintain the same mass flow in this case. This makes PFHS with CFDN VG to have less friction factor. THP is a function of heat transfer (Nu) and friction factor. Increase in Nu and reduction in friction factor by CFDN arrangement over CFU arrangement leads to 0.04 points increase in THP for PFHS with CFDN VG arrangement.

4.5 Comparison between bottom plate and vertical plate fin VGs
The results have shown that the vertical plate fin VG pair perform better than the bottom plate VGs. To understand this better, vorticity and temperature field values at 3 different axial locations are plotted in *Fig*. 17 and *Fig*. 18. As the vertical plate VG produces two pairs of

vortices, it leads to effective mixing of momentum and temperature of the fluid inside the channel compared to bottom plate VG, which produces a single pair of vortices. It can be observed that, bottom plate VG is not effective near the top region of the channel, this is indicated by the presence of cold fluid in the top region. The effective mixing of fluid temperature inside the channel by vertical plate VGs leads to increased heat transfer from the solid heat sink. This leads to a reduction in the heat sink's wall temperature, as shown in *Fig. 18*. Axial distribution of secondary flow intensity factor shows that (*Fig. 19*), the Se_{cs} of vertical plate fin VG is much higher than the bottom plate VG's Se_{cs} value, for the entire length of the channel. The Se_{cs} value integrated over the channel length for the vertical plate fin VG and bottom plate VG are $216368m^2$ and $106782m^2$ respectively. The high secondary flow has resulted in increased heat transfer by the vertical plate fin VG configuration.

The streamline pattern in *Fig. 20* shows that longitudinal vortices created by the vertical plate fin VG promote mixing for the whole height of the fluid channel, while in the bottom plate VG, vortices have not travelled to the top part of the fluid channel. So, mixing by bottom plate VG is limited to the lower half of the heat sink channel. This observation supports the improved performance of vertical plate VG relative to bottom plate VG.

4.6 Change in VG performance relative to velocity

 In order to calculate the change in performance of PFHS with VG relative to velocity (or Re), the best-performing bottom plate VG and vertical plate VG configuration, in CFU arrangement are evaluated at different inlet velocities. The variation of Nu, friction factor and THP with respect to Re are given in *Fig. 21* and Fig. *22* for PFHS with bottom plate VG and vertical plate VG configuration respectively. Nu increases as velocity or Re increases, and the friction factor and THP decreases as Re increases. THP depends on the ratio of Nu of PFHS with VG to Nu of

baseline PFHS (Eq. (8)). The Nu/Nu_s ratio decreases with increase in Re so is the f_s/f ratio. Hence the THP of PFHS also decreases with increase in Re. This trend indicates that VG's relative effectiveness decreases with increase in velocity. Further, the THP decrement rate against Re is higher for bottom plate VG than for vertical plate VG. Above Re=3400, VG gives a constant THP increment, i.e., vertical plate fin VG and bottom plate VG increase the THP by a constant amount of 15.9% and 8.2% respectively.

5. Conclusions

In this study, heat transfer characteristics of different delta winglet pair VG configurations mounted inside the PFHS channel were assessed. Two options to mount the VG on PFHS were considered: (i) bottom plate mounting and (ii) vertical plate fin mounting. For each mounting option, the effect of different design parameters on the heat transfer characteristics was evaluated through DoE based CFD simulations. The CFD setup and methodology were validated by comparing against the experimental results available in the literature. Based on the CFD results, the effect of each of the design parameters was evaluated, and polynomial response surface models have been developed for the Nu and THP of PFHS with VGs. The results show that,

i)   Bottom plate VG on PFHS improves the THP performance by 1.12 times (12%) compared to the baseline PFHS.

ii)   Vertical plate fin VG on PFHS improves the THP performance by 1.17 times (17%) compared to the baseline PFHS.

iii)   Vertical plate fin VG yields high performance than bottom plate VG. For the vertical plate fin VG, VG height is the most influential design variable. Positioning of the VG forwards is normally beneficial. If pressure drop concerns dominate, mounting the VG toward the rear is an appropriate compromise measure.

iv)   Delta winglet pair VG arranged in the CFDN configuration performs better than when arranged in the CFU configuration. This improvement stems from the increased heat

transfer and decreased friction factor by the CFDN configuration. The increment in THP is about 0.04 for the vertical plate fin VG at a flow velocity of 8m/s.

v)   The effect of gap length between the winglet pair trailing edges is evaluated for bottom plate VG, and it shows that as the gap length is decreased, velocity increases in the channel, and this helps in the heat transfer increment.

vi)   VGs continue to improve the heat transfer (Nu) as flow Re increases. Nu increases as Re increases but THP decreases with increasing Re. This is because the VG's relative effectiveness (Nu/Nu_s and f_s/f) decreases with increase in Re. The THP decrement against Re is higher for bottom plate VG than for vertical plate fin VG configuration.

6. Nomenclature

A_{HT} Total area of heat transfer surfaces (m^2)

CFD   Computational Fluid Dynamics

CFDN   Common Flow Down

CFU   Common Flow Up

Cp Specific heat capacity (J/kg/K)

D_h Hydraulic Diameter of PFHS channel (m)

DoE   Design of Experiments

f Friction factor

g Gap between winglet pair (m)

GCI Grid Convergence Index

h Height of delta winglet (m)

H_b	Height of PFHS bottom plate (m)
HTC	Heat Transfer Coefficient (W/m^2/K)
L	Length of delta winglet (m)
L_f	Length of plate fin (m)
LHC	Latin Hyper Cube
$\dot{m}$	Mass flow rate (kg/s)
Nu	Nusselt number
PFHS	Plate Fin Heat Sink
ΔP	Pressure difference between inlet and outlet (Pa)
R^2	Statistical measure of the accuracy of fitted regression model
Re	Reynolds number
Se	Secondary flow intensity factor
Se$_{cs}$	Secondary flow intensity averaged over a cross section
T	Temperature (K)
T_{ave}	Average of inlet and outlet temperature (K)
T_w	Averaged base plate temperature (K)
THP	Thermal Hydraulic Performance
u	Flow velocity (m/s)
VG	Vortex Generator
W_c	Channel width (m)

x	x-location of VG leading edge measured from heat sink's leading edge (m)
y_i	Response variable value
$\hat{y}_i$	Predicted value of response variables
$\bar{y}$	Mean value of all response variables

Greek symbols

α	Attack angle (deg)
β	Coefficients of response surface model
δ	Thickness of plate fin (m)
μ	Dynamic viscosity (Nsm^{-2})
ρ	Density (kg/m^3)
ω_n	Vorticity magnitude normal to the cross section (1/s)

Subscripts

ave	average
cs	Cross section
in	Inlet
out	Outlet
s	Baseline PFHS
w	wall

Acknowledgment

-

Funding

Nothing to declare.

Competing Interest

Nothing to declare.

7. References

[1] M. Fiebig, P. Kallweit, N. Mitra, and S. Tiggelbeck, "Heat transfer enhancement and drag by longitudinal vortex generators in channel flow", *Exp. Therm. Fluid Sci., vol. 4, no. 1, pp. 103-114*, Jan. 1991. DOI:10.1016/0894-1777(91)90024-L

[2] S.M. Pesteei, P.M.V. Subbarao, and R.S. Agarwal, "Experimental study of the effect of winglet location on heat transfer enhancement and pressure drop in fin-tube heat exchangers", *Appl. Therm. Eng., vol. 25, no. 11-12, pp. 1684-1696*, Aug. 2005. DOI: 10.1016/j.applthermaleng.2004.10.013

[3] J.M. Wu, and W.Q. Tao, "Numerical study on laminar convection heat transfer in a rectangular channel with longitudinal vortex generator. Part B, parametric study of major influence factors", *Int. J. Heat Mass Transf., vol. 51, no. 13-14, pp. 3683-3692*, 2008. DOI: 10.1016/j.ijheatmasstransfer.2007.03.031

[4] J.M. Wu, and W.Q. Tao, "Effect of longitudinal vortex generator on heat transfer in rectangular channels", *Appl. Therm. Eng., vol. 37, pp. 67-72,* 2012. DOI: 10.1016/j.applthermaleng.2012.01.002

[5] Y.-L. He, P. Chu, W-Q. Tao, Y-W. Zhang, and T. Xie, "Analysis of heat transfer and pressure drop for fin-and-tub heat exchangers with rectangular winglet-type vortex generators", *Appl. Therm. Eng., vol. 61, no. 2, pp.770–783*, Nov. 2013. DOI: 10.1016/j.applthermaleng.2012.02.040

[6] A. Sinha, H. Chattopadhyay, A.K. Iyengar, and G. Biswas, "Enhancement of heat transfer in a fin-tube heat exchanger using rectangular winglet type vortex generators", *Int. J. Heat Mass Transf., vol. 101, pp.667–681, Oct. 2016.* DOI: 10.1016/j.ijheatmasstransfer.2016.05.032

[7] A. Sinha, K.A. Raman, H. Chattopadhyay, and G. Biswas, "Effect of different orientations of winglet arrays on the performance of plate-fin heat exchangers," *Int. J. Heat Mass Transf., vol.57, no. 1, pp.202-214,* Jan. 2013. DOI: 10.1016/j.ijheatmasstransfer.2012.10.034

[8] G. Zhou, "Experimental investigations of heat transfer enhancement by plane and curved winglet type vortex generators with punched holes," *Int. J. Therm. Sci., vol. 78, pp. 26-35,* April 2014. DOI: 10.1016/j.ijthermalsci.2013.11.010

[9] M.K. Aliabadi, S. Zangouei, and F. Hormozi, "Performance of a plate-fin heat exchanger with vortex-generator channels: 3D-CFD simulation and experimental validation," *Int. J. Therm. Sci., vol. 88, pp. 180-192,* Feb. 2015. DOI: 10.1016/j.ijthermalsci.2014.10.001

[10] M. K. Aliabadi, O. Sartipzadeh, and A. Alizadeh, "An experimental study on vortex-generator insert with different arrangements of delta-winglets," *Energy, vol. 82, pp. 629–639,* 2015. DOI: 10.1016/j.energy.2015.01.072

[11] A. Datta, A. Das, P. Dey and D. Sanyal, "Multi objective optimization of laminar heat transfer and friction factor in rectangular microchannel with rectangular vortex generators: An application of NSGA II with gene expression programming metamodel," *J. Heat Transfer, vol. 139, no. 7,* Jul. 2017. DOI: 10.1115/1.4035890

[12] A. Abdollahi, and M. Shams, "Optimization of shape and angle of attack of winglet vortex generator in a rectangular channel for heat transfer enhancement," *Appl. Therm. Eng., vol. 81, pp.376–387,* April 2015. DOI: 10.1016/j.applthermaleng.2015.01.044

[13] M. Samadifar, and D. Toghraie, "Numerical simulation of heat transfer enhancement in a plate-fin heat exchanger using a new type of vortex generators," *Appl. Therm. Eng., vol. 133, pp. 671–681,* Mar. 2018. DOI: 10.1016/j.applthermaleng.2018.01.062

[14] A. Akcayoglu, and C. Nazli, "A comprehensive numerical study on thermohydraulic

performance of fluid flow in triangular ducts with delta-winglet vortex generators," *Heat Transfer Eng., vol. 39, no. 2, pp. 107-119*, Jan. 2018. DOI: 10.1080/01457632.2017.1288046

[15] H. E. Ahmed, and M. Z. Yusoff, "Thermal enhancement of triangular ducts using compound of vortex generators and nanofluids," *Heat Transfer Eng.,* 2017. DOI:10.1080/01457632.2017.1312874.

[16] A.T. Wijayanta, T. Istanto, K. Kariya, and A. Miyaro, "Heat transfer enhancement of internal flow by inserting punched delta winglet vortex generators with various attack angles", *Exp. Therm. Fluid Sci., vol. 87, pp. 141-148*, Oct. 2017. DOI: 10.1016/j.expthermflusci.2017.05.002

[17] A.T. Wijayanta, M. Aziz, K. Kariya, and A. Miyaro, "Numerical study of heat transfer enhancement of internal flows using double-sided delta winglet tape insert*", Energies, vol. 11, 3170*, Nov. 2018. DOI: 10.3390/en11113170

[18] K. Song et al., "Effect of geometric size of curved delta winglet vortex generators and tube pitch on heat transfer characteristics of fin-tube heat exchanger", *Exp. Therm. Fluid Sci., vol. 82, pp. 8-18*, April 2017. DOI: 10.1016/J.EXPTHERMFLUSCI.2016.11.002

[19] K. Song, and T. Tagawa, "Optimal arrangement of vortex generators for best heat transfer enhancement in flat-tube-fin heat exchanger", *Int. J. Therm. Sci., vol. 132, pp. 35-367*, Oct. 2018. DOI: 10.1016/j.ijthermalsci.2018.06.011

[20] K. Yang, J. Jhong, Y. Lin, K. Chien, and C. Wang, "On the heat transfer characteristics of heat sinks: with and without vortex generators," *IEEE Trans. Compon. Packaging Manuf. Technol., vol. 33, no. 2, pp. 391-397*, Jun. 2010. DOI: 10.1109/TCAPT.2010.204441

[21] H. Y. Li, C. Chen, S. Chao, and G. Liang, "Enhancing heat transfer in a plate fin heat sink using delta winglet vortex generators," *Int. J. Heat Mass Transf., vol. 67, pp. 666-677,* Dec. 2013. DOI: 10.1016/j.ijheatmasstransfer.2013.08.042

[22] H.Y. Li, W. Liao, T. Li, and Y. Chang, "Application of vortex generators to heat transfer enhancement of a pin-fin heat sink," *Int. J. Heat Mass Transf., vol. 112, pp. 940–949*, Sep. 2017. DOI: 10.1016/j.ijheatmasstransfer.2017.05.032

[23] H.E. Ahmed, "Optimization of thermal design of ribbed flat-plate fin heat sink," *Appl. Therm. Eng., vol. 102, pp. 1422-1432,* Jun. 2016. DOI: 10.1016/j.applthermaleng.2016.03.119

[24] Y. T. Yang, and P. J. Chen, "Numerical optimization of turbulent flow and heat transfer characteristics in a ribbed channel," *Heat Transfer Eng.,* vol. 36, no. 3, pp. 290–302, 2015. DOI: 10.1080/01457632.2014.916158

[25] N. Sharma, A. Tariq and M. Mishra, "Experimental Investigation of Heat Transfer Enhancement in Rectangular Duct with Pentagonal Ribs," *Heat Transfer Eng.*, vol. 40, no.1-2, pp. 147-165, 2019. DOI: 10.1080/01457632.2017.1421135

[26] H. Liu, C. Fan, Y. He, and D.S. Nobes, "Heat transfer and flow characteristics in a rectangular channel with combined delta winglet inserts," *Int. J. Heat Mass Transf., vol. 134, pp. 149-165,* May. 2019. DOI: 10.1016/j.ijheatmasstransfer.2019.01.004

[27] K. Song, T. Tagawa, Z. Chen, and Q. Zhang, "Heat transfer characteristics of concave and convex curved vortex generators in the channel of plate heat exchanger under laminar flow," *Int. J. Therm. Sci., vol. 137, pp. 215-228,* Mar. 2019. DOI: 10.1016/j.ijthermalsci.2018.11.002

[28] E. Ali, J. Park, and H. Park, "Numerical investigation of enhanced heat transfer in a rectangular channel with winglets", *Heat Transfer Eng.*, vol. 42, no. 8, pp. 695-705, 2021. DOI: 10.1080/01457632.2020.1723845

[29] H. Naik, and S. Tiwari, "Effect of winglet location on performance of fin-tube heat exchangers with inline tube arrangement," *Int. J. Heat Mass Transf., vol. 125, pp. 248-261*, Oct. 2018. DOI: 10.1016/j.ijheatmasstransfer.2018.04.071

[30] H. Naik, S. Harikrishnan, and S. Tiwari, "Numerical investigations on heat transfer characteristics of curved rectangular winglet placed in a channel," *Int. J. Therm. Sci., vol. 129*, pp. 489-503, Jul. 2018. DOI: 10.1016/j.ijthermalsci.2018.03.028

[31] M. Awais, and A. Bhuiyan, "Enhancement of thermal and hydraulic performance of compact finned-tube heat exchanger using vortex generators (VGs): A parametric study," *Int. J. Therm. Sci., vol. 140, pp. 154-166,* Jun. 2019. DOI: 10.1016/j.ijthermalsci.2019.02.041

[32] Z. Chamanroy and M.K. Aliabadi, "Analysis of straight and wavy miniature heat sinks equipped with straight and wavy pin-fins", *Int. J. Therm. Sci., vol.146, 2019.* DOI.org/10.1016/j.ijthermalsci.2019.106071

[33] E. Hosseinirad, M.K. Aliabadi, and F.Hormozi, "Effects of splitter shape on thermal-hydraulic characteristics of plate-pin-fin heat sink", *Int. J. Heat Mass Transf., vol.143, 2019.* DOI.org/10.1016/j.ijheatmasstransfer.2019.118586

[34] M.K. Aliabadi, A. Abbaszadeh, M.M. Rashidi, "Comparison of co and counter current modes of operation for wavy mini channel heat sinks", *Int. J. Therm. Sci., vol.171, 2022.* DOI.org/10.1016/j.ijthermalsci.2021.107189

[35] H.E. Ahmed, H.A. Mohammed, and M.Z. Yusoff, "An overview on heat transfer augmentation using vortex generator and nano fluids: Approaches and applications," *Renew. Sust. Energ. Rev., vol. 16, no. 8, pp. 5951-5993*, Oct. 2012. DOI: 10.1016/j.rser.2012.06.003

[36] N. Zheng, F. Yan, K. Zhang, T. Zhou, and Z. Sun, "A review on single-phase convective heat transfer enhancement based on multi-longitudinal vortices in heat exchanger tubes," *Appl. Therm. Eng., vol. 164, pp. 114475*, Jan. 2020. DOI: 10.1016/j.applthermaleng.2019.114475

[37] M. Santhanakrishnan, T. Tilford, and C. Bailey, Multi-material heat sink design using level-set topology optimization, *IEEE Trans. Compon. Packaging Manuf. Technol., vol. 9, no. 8,* Aug.

2019. <u>DOI: 10.1109/TCPMT.2019.2929017</u>.

[38] M. Santhanakrishnan, T. Tilford, and C. Bailey, Multi-objective NSGA-II based shape optimisation of the cross-sectional shape of passively cooled heat sinks, *Int. J. Numer. methods heat fluid flow, vol.32, no.3, pp.1025-1045*, Jan.2022. <u>DOI:10.1108/HFF-10-2020-0656</u>

[39] H. Jonsson and B. Moshfegh, "Modeling of the thermal and hydraulic performance of plate fin, strip fin and pin fin heat sinks – Influence of flow bypass," *IEEE Trans. Compon. Packaging Manuf. Technol.., vol. 24, no. 2,* Jun. 2001. <u>DOI: 10.1109/6144.926376</u>

[40] F. Zhou and I. Catton, "Numerical evaluation of flow and heat transfer in plate-pin fin heat sinks with various pin cross-sections," *Numer. Heat Tr. A-appl.*, vol. 60, no. 2, pp.107-128, Jul. 2011. <u>DOI: 10.1080/10407782.2011.588574</u>

[41] R.W. Hanks and H.C. Ruo, "Laminar-turbulent transition in ducts of rectangular cross section" *Industrial and Engineering Chemistry fundamentals*, vol.5, no.4, 1966.

[42] F.R. Menter, "Two-equation eddy-viscosity turbulence models for engineering applications", *AIAA J., vol. 32, no. 8, pp. 1598-1605*, Aug. 1994. <u>DOI: 10.2514/3.12149</u>

[43] P.J. Roache, "Quantification of uncertainty in computational fluid dynamics," *Annu. Rev. Fluid Mech., vol. 29, no. 1, pp. 123–160*, 1997. <u>DOI: 10.1146/annurev.fluid.29.1.123</u>

[44] J.F. Fan, W.K. Ding, J.F.Zhang, Y.L. He, W.Q. Tao, "A performance evaluation plot of enhanced heat transfer techniques oriented for energy saving", *Int. J. Heat Mass Transf., vol.52, pp. 33-44. 2009.* <u>DOI.org/10.1016/j.ijheatmasstransfer.2008.07.006</u>

[45] K. Song, and L.B. Wang, "The effectiveness of secondary flow produced by vortex generators mounted on both surfaces of the fin to enhance heat transfer in a flat tube bank fin heat exchanger", *J. Heat Transfer, vol. 135, no. 4, pp. 041902-11*, Apr. 2013. <u>DOI: 10.1115/1.4023037</u>

[46]J.M. Wu, and W.Q. Tao, "Numerical study on laminar convection heat transfer in a rectangular channel with longitudinal vortex generator. Part A: Verification of field synergy principle", *Int. J. of Heat Mass Transfer, vol.51, pp. 1179-1191, 2008.* DOI:10.1016/j.ijheatmasstransfer.2007.03.032

Table 1 Geometric details of PFHS

Parameter	Value (m)	Parameter	Value(m)
Length of plate fin (L_f)	0.051	Height of the fin (H_f)	0.01
Height of the base (H_b)	0.003	Channel width (W_c)	0.005
Plate fin thickness (δ)	0.0015		

Table 2 Properties of Air and Aluminium

	Air	Aluminium
Density (kg/m3)	1.225	2719
Temperature (K)	293.1 (Inlet)	-
Viscosity	1.789e-5	-
Thermal conductivity (W/m-k)	0.0242	202.4
Specific heat capacity (J/kg-K)	1006.43	871

Table 3 Design variables limit for a) Bottom plate VG and b) Vertical plate fin VG

Bottom plate VG	Minimum	Maximum	Difference
L (m)	0.0015	0.0065	0.005
h/L	0.3	1	0.7
x/L_f	0.05	0.7	0.65

(a)

Vertical plate fin VG	Minimum	Maximum	Difference
h (m)	0.001	0.00225	0.00125
Attack angle	8º	30º	22º
L/h	1	6	5
x/L_f	0.02	0.6	0.58

(b)

Table 4 Bottom plate VG performance for different gap lengths between delta winglet trailing edges

Gap length	Nu	THP
0.002m	217.736	1.0952
0.001m	237.369	1.1216

Table 5 Coefficient values of model equation corresponding to Nu and THP for bottom plate VG

	Nu	THP		Nu	THP
β_o	172.0282	1.0273	β_6	7.9555	0.0110
β_1	22.8448	0.0072	β_7	36.2665	0.0313
β_2	38.6685	0.0718	β_8	-14.2492	-0.0326
β_3	-3.0572	-0.0151	β_9	-27.6130	-0.0808
β_4	14.2414	0.0839	R^2 statistic (%)	97.47	82.42
β_5	-21.3539	-0.0991			

Table 6 Coefficient values of model equation corresponding to Nu and THP for vertical plate fin VG

	Nu	THP		Nu	THP
β_o	177.8368	1.0229	β_8	-15.1524	-0.2227
β_1	4.0634	-0.0909	β_9	49.1266	0.0359
β_2	10.8775	0.0024	β_{10}	19.5112	-0.0355
β_3	25.3250	0.1484	β_{11}	7.0196	0.1673
β_4	22.4430	0.2017	β_{12}	-49.0778	-0.2033
β_5	16.8529	0.1452	β_{13}	44.7131	0.1125
β_6	-12.1765	0.0305	β_{14}	-5.3064	0.0432
β_7	-32.3850	-0.1987	R^2 statistic (%)	99.98	98.13

Table 7 Comparison of CFDN and CFU VG configurations

Type	Nu	Friction factor	THP
CFU	256.125	0.2225	1.1719
CFDN	261.733	0.2146	1.2121

Figure Captions List

Fig. 1   PFHS geometry

Fig. 2   PFHS with bottom plate VG

Fig. 3   PFHS with vertical plate fin VG

Fig. 4   Computational domain used for the study with the heat sink geometry

Fig. 5   a) Mesh details b) Grid independence study

Fig. 6   Convergence history of CFD simulations

Fig.7   Validation of CFD modelling by comparing against experimental data of [39]

Fig.8   Temperature (K) distribution at x/L_f=0.44 and 0.64 on PFHS with bottom plate VG pair gap length=2mm (left) and 1mm (right)

Fig.9   Velocity(m/s) distribution at x/L_f=0.44 and 0.64 on PFHS with bottom plate VG pair gap length=2mm (left) and 1mm (right)

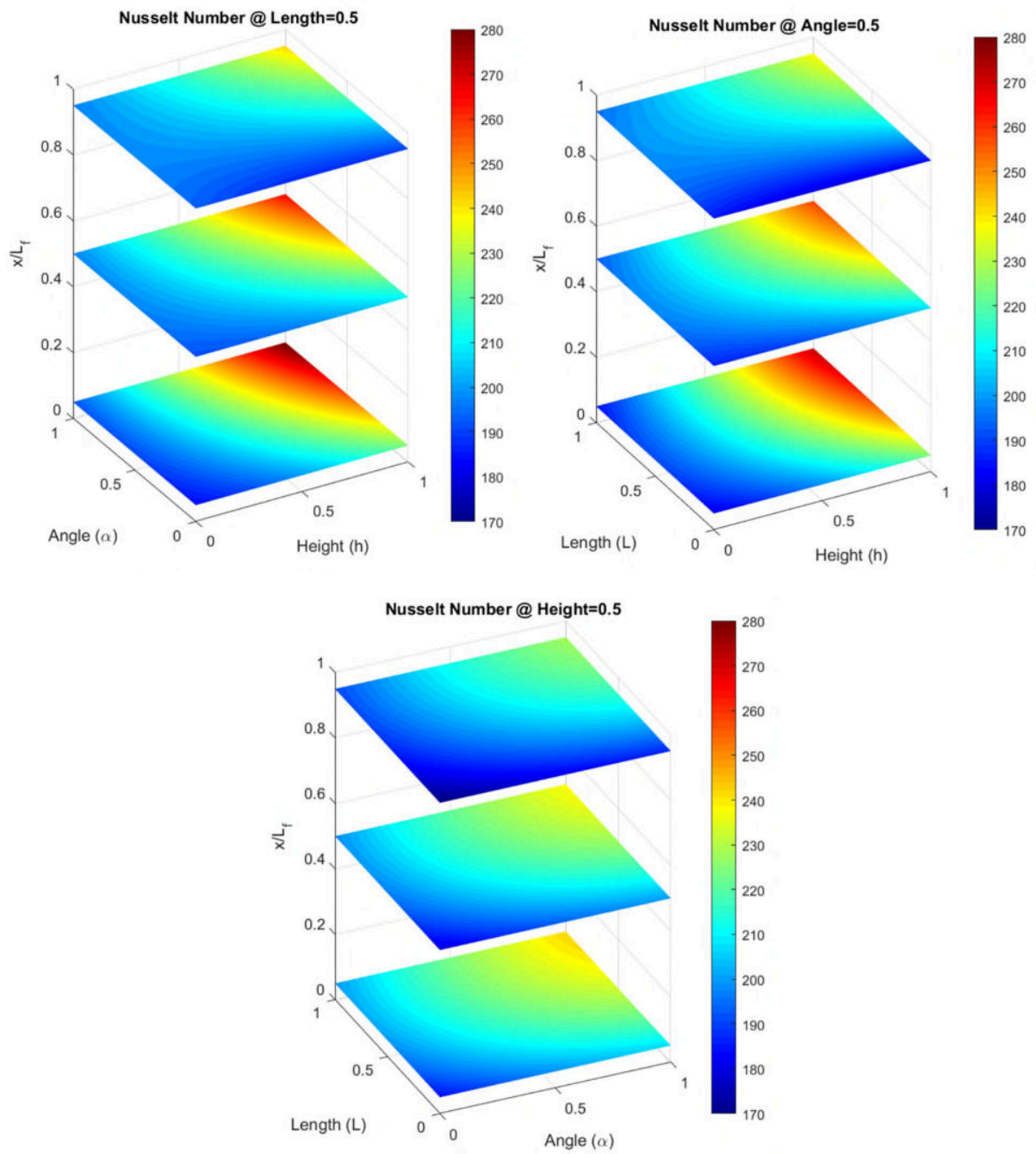Fig.10   Variation of Nu and THP of bottom plate VG with respect to different design parameters

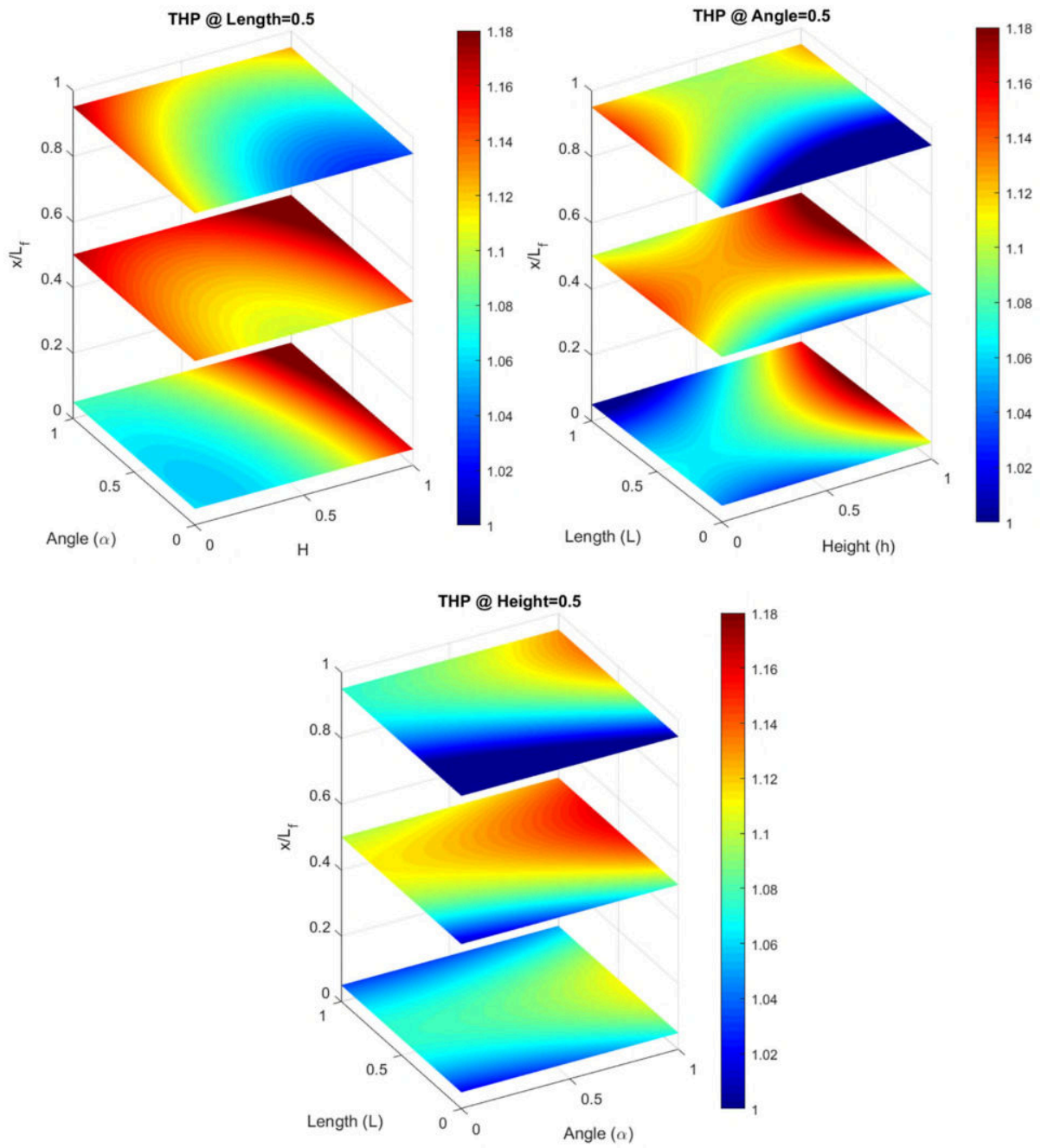Fig.11   Variation of Nu with respect to different design parameters of vertical plate fin VG

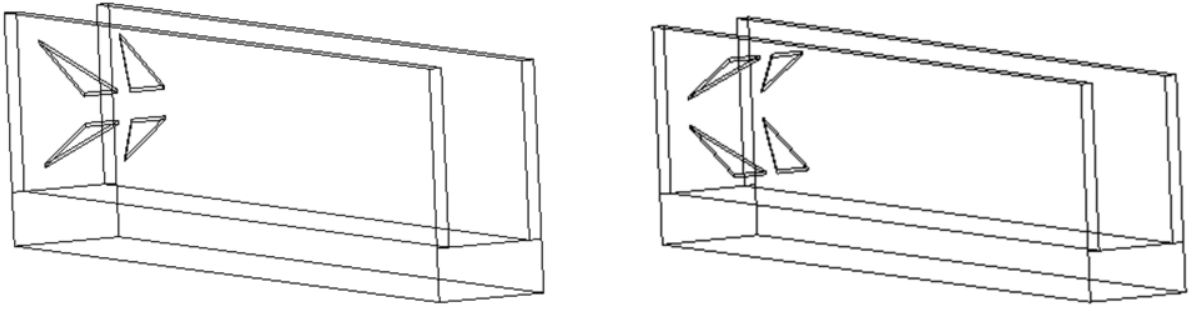Fig.12   Variation of THP with respect to different design parameters of vertical plate fin VG

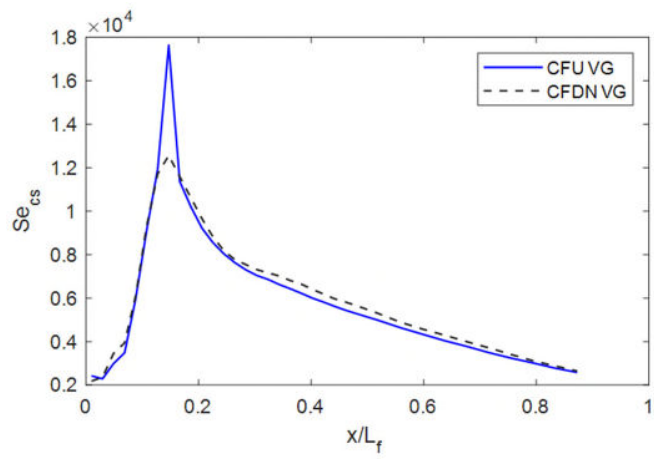Fig.13   PFHS with CFU (left) and CFDN (right) configuration VGs

Fig. 1 PFHS geometry

Fig. 2 PFHS with bottom plate VG

Fig. 3 PFHS with vertical plate fin VG

Fig. 4 Computational domain used for the study with the heat sink geometry

(a)   (b)

Fig. 5 a) Mesh details b) Grid independence study

Fig. 6 Convergence history of CFD simulations

Fig. 7 Validation of CFD modelling by comparing against the experimental data of [39]

Fig. 8 Temperature (K) distribution at x/L$_f$=0.44 and 0.64 on PFHS with bottom plate VG pair gap length=2mm (left) and 1mm (right)

Fig. 9 Velocity(m/s) distribution at x/L$_f$=0.44 and 0.64 on PFHS with bottom plate VG pair gap length=2mm (left) and 1mm (right)
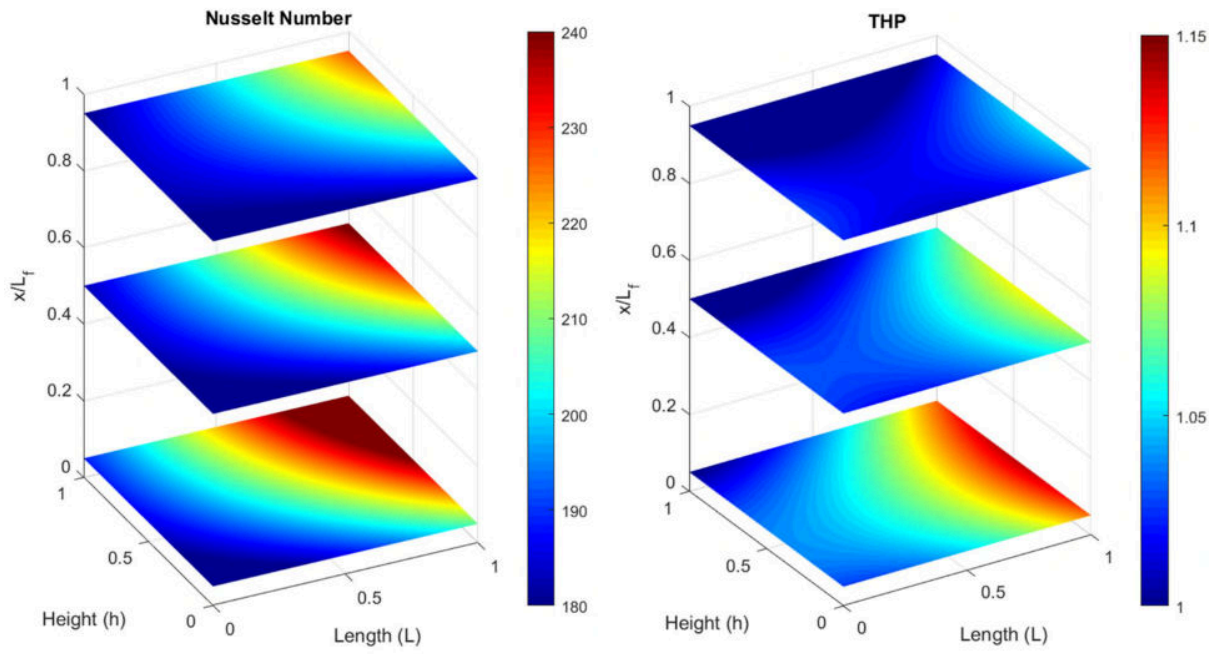
Fig. 10 Variation of Nu and THP of bottom plate VG with respect to different design parameters

Fig. 11 Variation of Nu with respect to different design parameters of vertical plate fin VG

Fig. 12 Variation of THP with respect to different design parameters of vertical plate fin VG

Fig. 13 PFHS with CFU (left) and CFDN (right) configuration VGs

Fig. 14 Secondary flow intensity distribution for vertical fin VG in CFU and CFDN arrangement
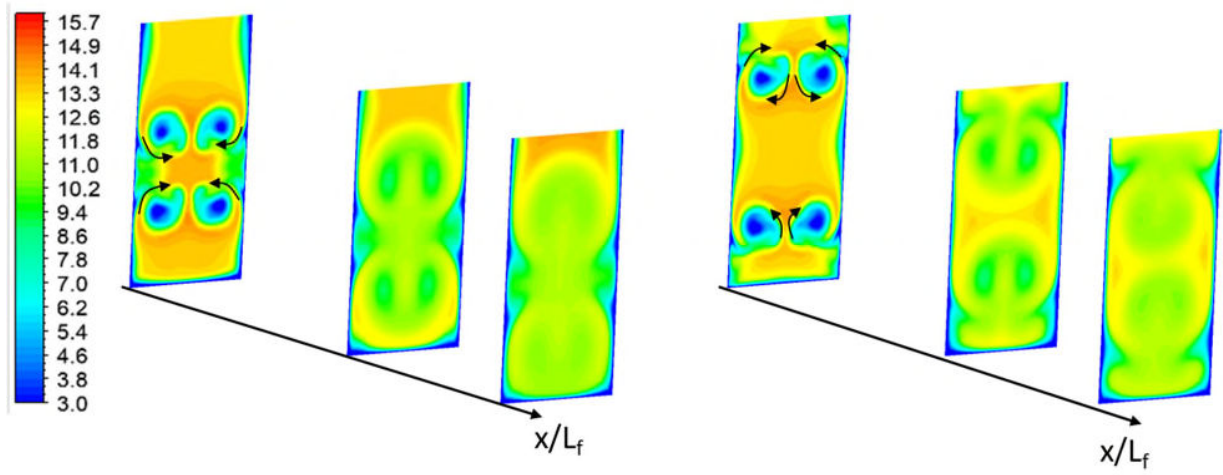
Fig. 15 Velocity (m/s) field at x/L$_f$=0.18, 0.46 and 0.66 on CFU (Left) and CFDN VG (Right) on PFHS
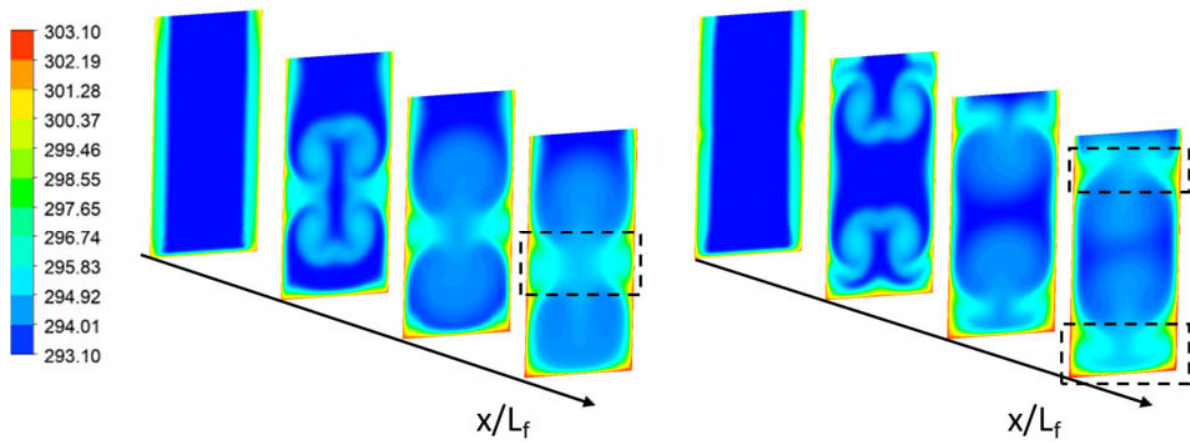
Fig. 16 Temperature (K) field at x/L$_f$ =0.06, 0.26, 0.46 and 0.66 on CFU (Left) and CFDN VG (Right) on PFHS
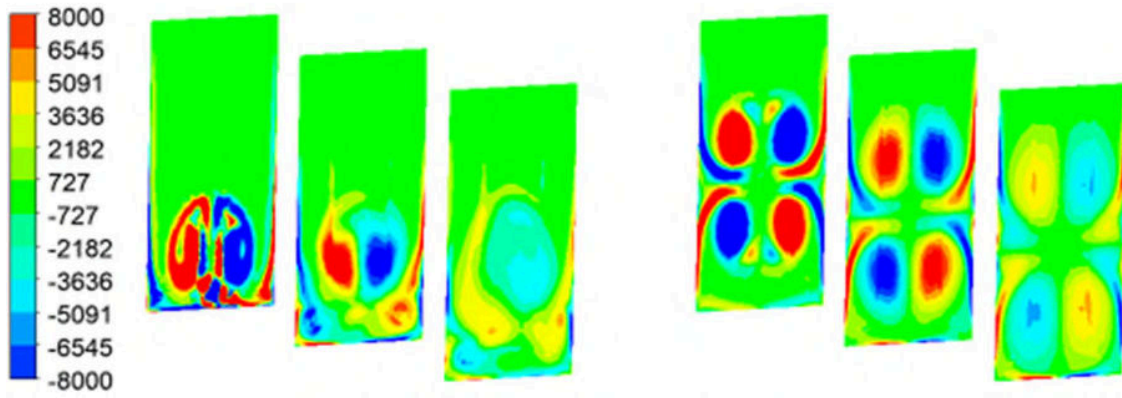
Fig. 17 x-Vorticity (1/s) field at x/L$_f$=0.26, 0.46 and 0.66 for bottom plate VG and vertical plate fin VG
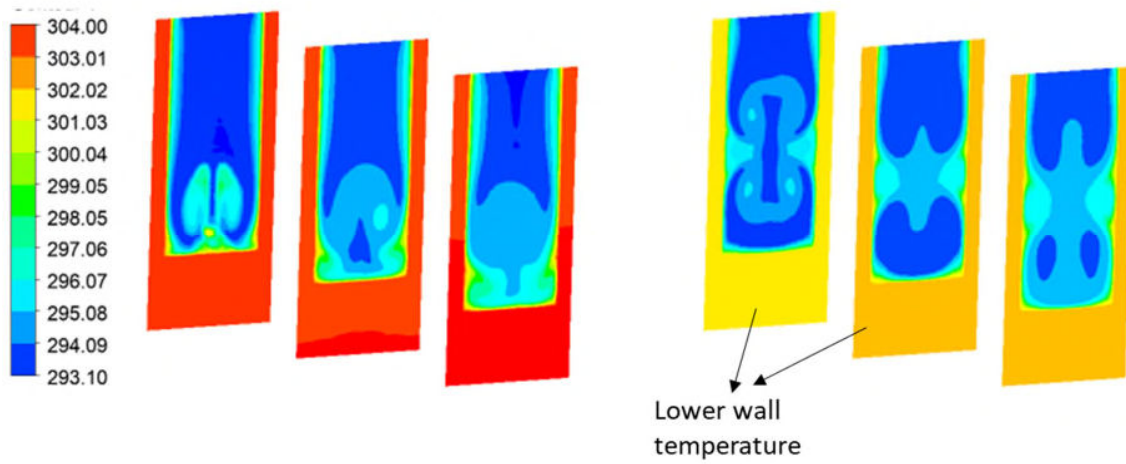
Fig. 18 Temperature(K) field at x/L$_f$=0.26, 0.46 and 0.66 for bottom plate VG and vertical plate fin VG
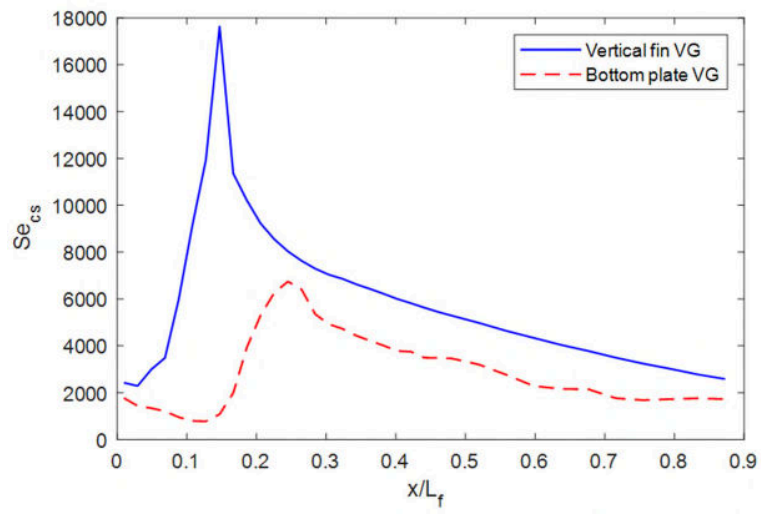
Fig. 19 comparison of secondary flow intensity distribution between PFHS with vertical fin VG and bottom plate VG
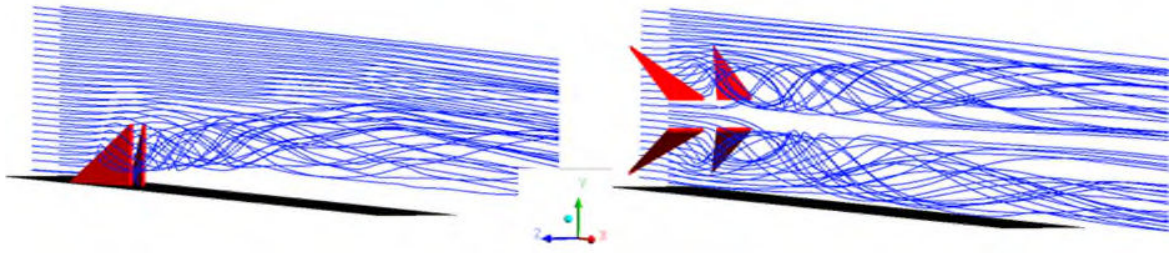
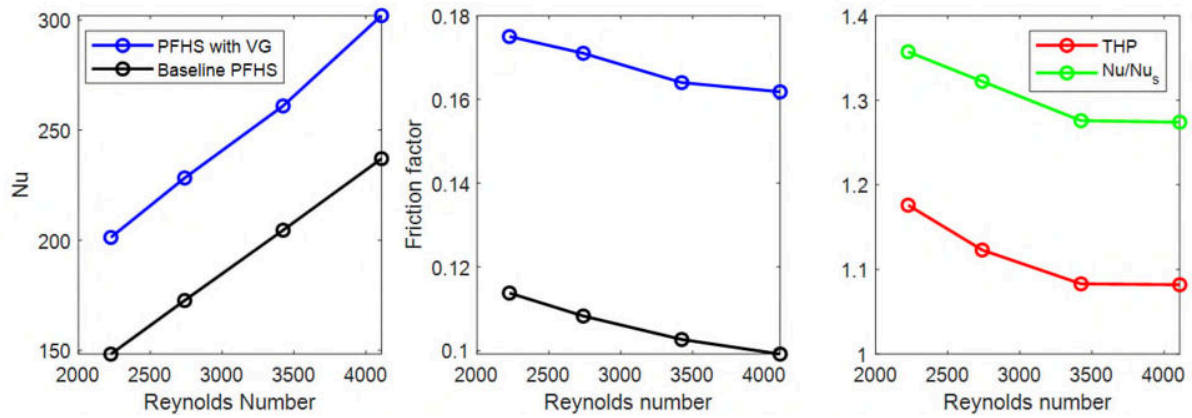Fig. 20 Flow pattern over the bottom plate VG and vertical plate fin VG

Fig. 21 Variation of Nu, Friction factor and THP relative to Re for PFHS with bottom plate VG in CFU arrangement
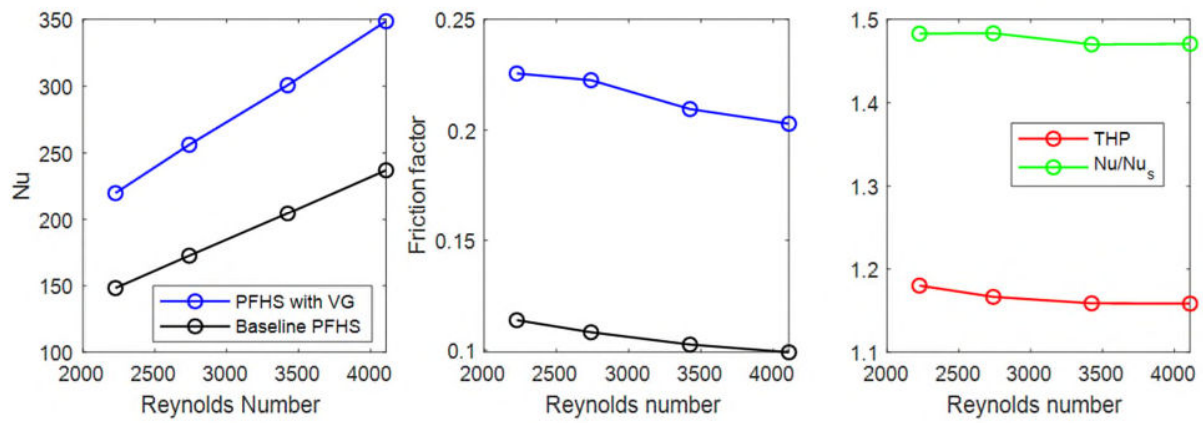
Fig. 22 Variation of Nu, Friction factor and THP relative to Re for PFHS with vertical plate VG in CFU arrangement